

Fermilab

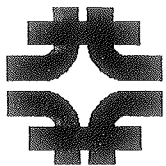
SDC Solenoid Design Note #149

Title: Radial and Axial Decentering Forces for Several SDC Solenoid/Calorimeter Configurations

AUTHOR: B. Wands

DATE: July 26, 1991

ABSTRACT: Radial and axial decentering forces are calculated for four generic test cases representing a range of distances between endplug and coil. A coil installation within 1 inch of the magnetic center of the iron is assumed. Two dimensional finite element models are used. The technique of calculating radial decentering from a two dimensional model is verified with three dimensional comparisons. The results show that geometries with endplugs extending into the bore of the solenoid produce large radial and axial forces, as expected, with the radial forces being particularly high.



Radial and Axial Decentering Forces for Several SDC Solenoid/Calorimeter Configurations

Bob Wands

Introduction

Imprecision in the placement of the solenoid within its return iron will result in field asymmetries and subsequent forces in the axial and radial directions. The purpose of this report is to calculate these forces for four of the SDC solenoid/calorimeter generic test case configurations⁽¹⁾

Solenoid/Calorimetry Configurations

The four generic test case configurations are shown in Fig. 1. Case 0 has a reentrant endplug which extends 40 cm. into the solenoid bore. Case 2 has an endplug which ends 40 cm. outside of the bore. Case 7 is identical to Case 0 except that an annular region of the outer radius of the reentrant endplug portion corresponding to approximately one tower has been eliminated to increase the air between the endplug and coil. Case 9 is similar to Case 2, except the endwall is now 1.23 m from the end of a current sheet which is also shorter than that of the first two configurations. Case 9 closely resembles an iron-free coil.

In all four cases the calorimetry is also the flux return, and is modeled as 1/4 in slots of air in two inch iron plates.

Analytical Approach

The finite element models of Ref. 1 were axisymmetric, and half-length, and modeled the slotted air/iron endplugs exactly. This led to a large number of elements. The modeling of the slots in three dimensions is prohibitive, and smearing the B-H properties in a rational way to approximate the slots does not seem possible in regions where the flux may travel either parallel or perpendicular to the slots. Therefore, the existing 2-d axisymmetric models were modified as described below to simulate off-center installation in the magnet iron.

Axial Decentering

This calculation was made by first solving the model for a current sheet of actual length. Then the current sheet was lengthened in the axial direction a total of 2 cm. The axial compressive forces from each run, calculated by the ANSYS program from the current density and the field solution, were subtracted from each other to produce the net axial force difference. It was assumed that the force increment at one end resulting from the lengthening of the current sheet would be equal and of the same sign at the other end of the solenoid where the current sheet was effectively shortened by a off-center placement. So, the total axial decentering force was found by multiplying the net axial force difference between the two models by two. This method has been checked against the more precise calculation using a 2-d, axisymmetric model of the entire length of the solenoid, and found to be within 5% of the full length result.

Radial Decentering

This calculation was made by first solving the model with the current sheet and iron in their radially centered locations. Then, another run was made in which the iron was moved radially inward a total of 2 cm. The difference in radial force on each coil element between the two runs was calculated. This force difference was then used to calculate the radial decentering force as detailed in Appendix A.

To verify this approach, the simplified solenoid/iron geometry of Fig. 2 was modeled in both two and three dimensions. The method just mentioned was applied to the 2-d model (Fig. 3) to determine the radial force. The three dimensional models allowed the actual displacement of the coil. The following 3-d models and methods were used in the verifications:

1. Difference scalar potential (DSP) coarse mesh of 1/4 of solenoid. This model, shown in Fig. 4, was intended primarily to produce boundary conditions for a more refined model of the coil region. The method of virtual work, as internally performed by ANSYS, was used to calculate the forces on the coil.
2. Difference scalar potential, refined mesh in region of the coil. This is shown in Fig. 5. This model used the boundary conditions from the coarse DSP mesh and the method of virtual work for force calculation.

3. Vector potential (VP) coarse mesh of 1/4 of solenoid. This is shown in Fig. 6. This model was intended for used with a refined model in the same manner as 1) and 2). The forces are available from ANSYS as Lorentz forces calculated in each coil element.
4. Vector potential refined mesh in region of coil, shown in Fig. 7. This model used the boundary conditions from the coarse VP mesh, and produced coil forces as Lorentz forces.
5. Difference scalar potential with total energy difference. This method uses coarse meshes of both a displaced and centered coil, and looks at the energy difference between the two.
6. Vector potential with total energy difference. Same as 5) but with uses the VP coarse mesh models.

The resulting forces are shown in Table I. Of the six methods used, the VP and DSP refined methods give very similar results, and agree well with the approximate 2-d method. The total energy difference technique fails, probably due to the very small energy difference resulting from a 2 cm coil displacement (about 1 part in 100000) which is too small to calculate with sufficient precision. The DSP coarse model was never intended to provide accurate results, but merely boundary conditions for the refined DSP model. The VP results are surprisingly similar between coarse and refined models.

Plots were made of the axial field component in the coil to compare the various models. Fig. 8 shows the axial component at the coil mean radius, as calculated at the element centroid, for the case of a centered coil. The DSP model shows considerable "noise", probably due to the numerical integration which is used to calculate the current source contribution to field. The 2-d and 3-d vector potential methods agree well.

Fig. 9 compares the axial field at the coil mean radius in the 3-d displaced submodels to the axial field of the 2-d model with the iron boundary moved in 2 cm. The close agreement between the 3-d vector potential and the 2-d vector potential indicates that the 2-d method of moving the iron boundary produces accurate field results for the region of coil which has displaced 2 cm toward the iron.

Comparison with CDF Calculations

The method of calculating radial forces from the 2-d models was applied to the CDF solenoid, using a detailed model available from a previous analysis. The resulting force was 5 tonnes/in, compared with 30 tonnes/in as reported by R. Yamada ⁽²⁾

This work suggests that the 2-d method is accurate enough for radial force calculation.

Results

The radial and axial decentering forces as calculated by the described methods for the four cases are given in Table II. A displacement of 1 inch from the nominally centered position is assumed. Although the term decentering is used, it is true that while all axial forces are decentering (force tends to increase in the direction of displacement), the radial forces for generic case 0 and 7 are in fact centering forces. From the standpoint of design, there is no use in distinguishing between centering and decentering; The coil must be held in its' as-installed location regardless.

Discussion

The largest forces occur for geometries where iron is close to the coil, as expected. The extension of iron 0.4 m into the bore of the solenoid (Case 0 and Case 7) produces large radial forces. Case 2, with the iron terminated 0.4 outside the solenoid bore, shows much less sensitivity. Case 0 was run primarily to determine if the deletion of the tower represented by Case 7 was the primary cause of the large radial force; It was not. The sensitivity of the radial force to the presence of iron in the solenoid bore argues for geometries which avoid this feature, especially in view of the more massive support structure required to resist the force.

References

1. Wands, B., "Magnetostatic Analysis of Several SDC Solenoid/Calorimeter Configurations". SDC Solenoid Design Note #138, March, 1991.
2. Fast, R., et. al., Design Report for an Indirectly Cooled 3-m Diameter Superconducting Solenoid for the Fermilab Collider Detector Facility, Fermilab TM-1135, October, 1982.

Appendix A

Calculation of Radial Decentering Force from a 2-d Finite Element Model

The object of the calculation is to represent the phi variation of radial B-field component with an axisymmetric model. Since the model will be by nature invariant in phi, it is necessary to use at least two models. The simplest approach might be to perform one run with a coil radius of $r_m + d$, and another run with a coil radius of r_m , where r_m is the actual coil radius and d is the desired decentering. Each run produces a set of Lorentz forces (in N/rad) and the assumption can be made that the difference in these forces represents the attraction to (or repulsion from) the iron at the phi corresponding to the closest iron/coil distance. Reversing the sign on these forces will give the repulsion from (or attraction to) the iron at a phi 180 degrees away. The forces in between can then be calculated by interpolating between the two extremes in some rational way.

The primary problem with the approach of increasing coil radius to represent decentering is that the act of increasing radius will by itself increase force. This is apparent from the magnetic pressure analogy applied to the inner coil surface. The hoop stress in the coil is

$$S_h = P_m r_m / t$$

where P_m is the magnetic pressure, $B^2 / (2 * \mu_0)$, and t is the coil thickness. Any increase in r_m increases S_h , regardless of any iron effects, assuming the change in B-field is small. Also, although intuition indicates that the desired decentering forces result from the variation of axial field component near the end of the coil, the method of increasing coil radius will produce higher forces all along the solenoid length. The results can be very large (conservative) decentering forces. The experience with this work was that the effects of reentrant iron were in fact nearly washed out by the large decentering forces calculated in this way.

It is more accurate and intuitively pleasing to move the iron boundary instead of the coil to represent the decentered coil. The two sets of forces are then used as previously stated to find the total decentering.

The selection of an interpolation scheme was somewhat arbitrary. Referring to Fig. A1, the radial force acting on the coil can be assumed to be inversely proportional to the square of the distance d . The force difference from the finite element runs F_{fea} (N/rad) is assumed to exist only at $\theta = 0$ and $d = 0$. At $\theta = 0$ and $d = 0.02$ m, the force difference is assumed to be zero. This pattern is assumed to exist in all four quadrants of the cross section, with the signs of the force difference reversed in the third and fourth quadrant. Then, at any θ , the force difference in the first quadrant is

$$F = F_{fea}(0.02-d)^2 \sin(\theta)/(0.02)^2$$

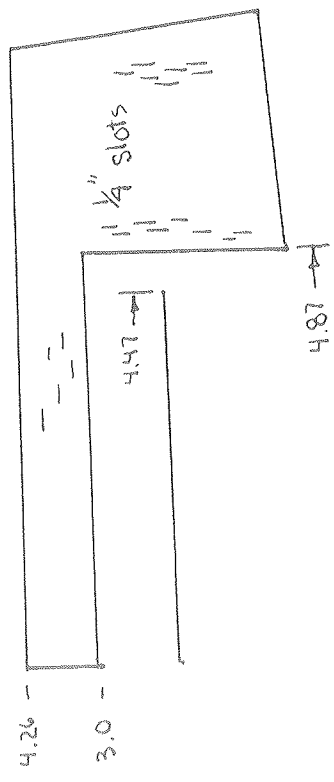
The distance d can be expressed in terms of r_1 as shown in the figure. This expression is numerically integrated in the first quadrant, then multiplied by four to obtain the total radial force. Note that this method does not consider the axial distribution of the force difference, but sums the force difference in all elements along the axis at a given θ .

Table I.
Radial Force Comparison

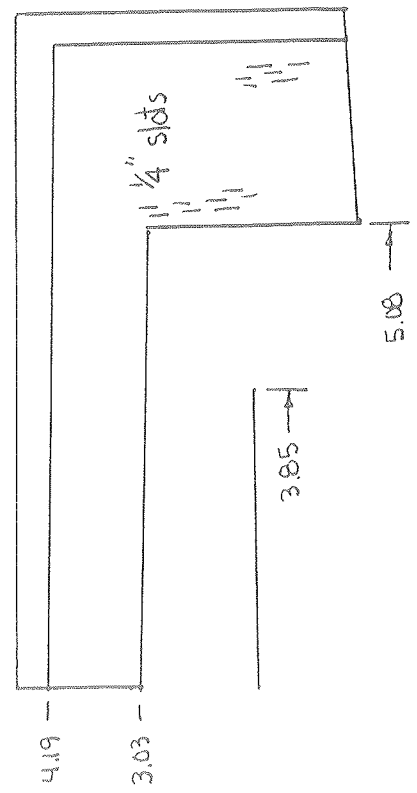
Model	Radial Force (tonnes/2 cm)
DSP - 3d (coarse)	3.3
V - 3d (coarse)	11.0
DSP - 3d (refined)	12.1
V - 3d (refined)	11.1
DSP - 3d (total energy)	5.4
V - 3d (total energy)	20.1
V__2d approximate	11.1

Table II
Axial and Radial Decentering Forces
for Four Generic Cases

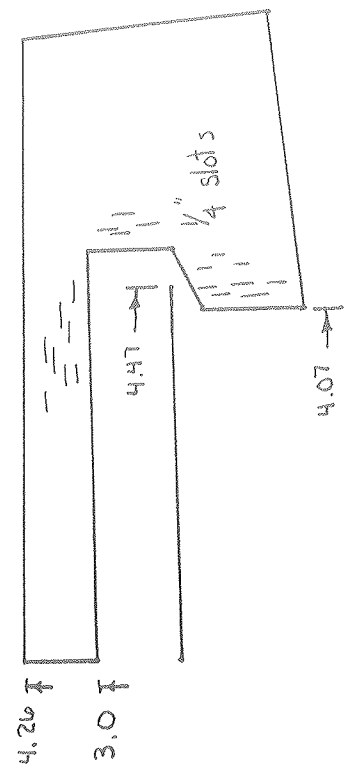
Case	Axial Decentering Force (tonnes/in)	Radial Decentering Force (tonnes/in)
0	-	206
2	43	<1
7	66	200
9	5	<1



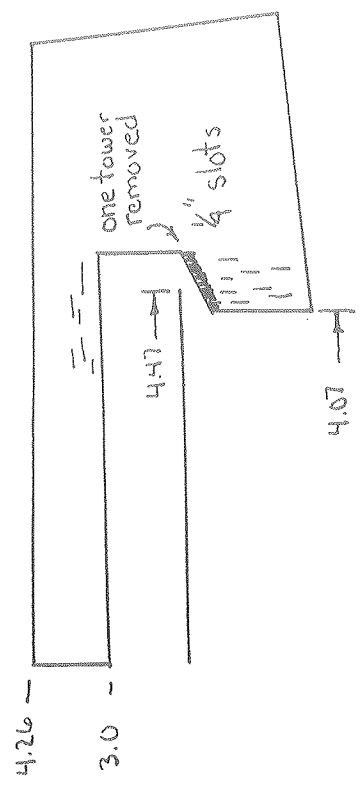
Case 2



Case 9



Case 0



Case 7

Fig. 1. Coil/Calorimeter Geometries

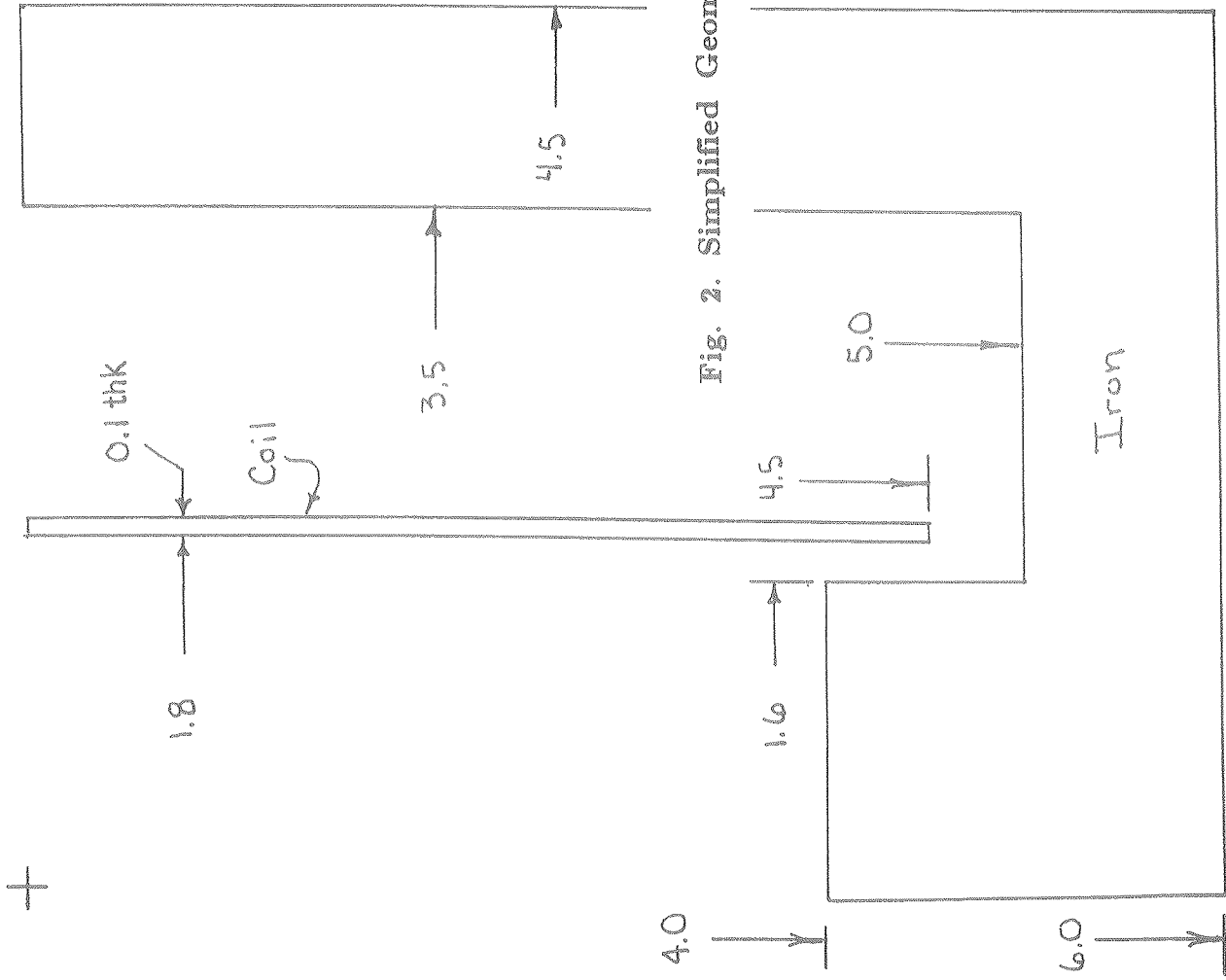


Fig. 2. Simplified Geometry for Radial Decentering Verification

ANSYS 4.4A
JUL 18 1991
9:51:23
PLOT NO. 1
PREP7 ELEMENTS
TYPE NUM
ZV = 1
DIST=3.3
XF =2.25
YF =-3

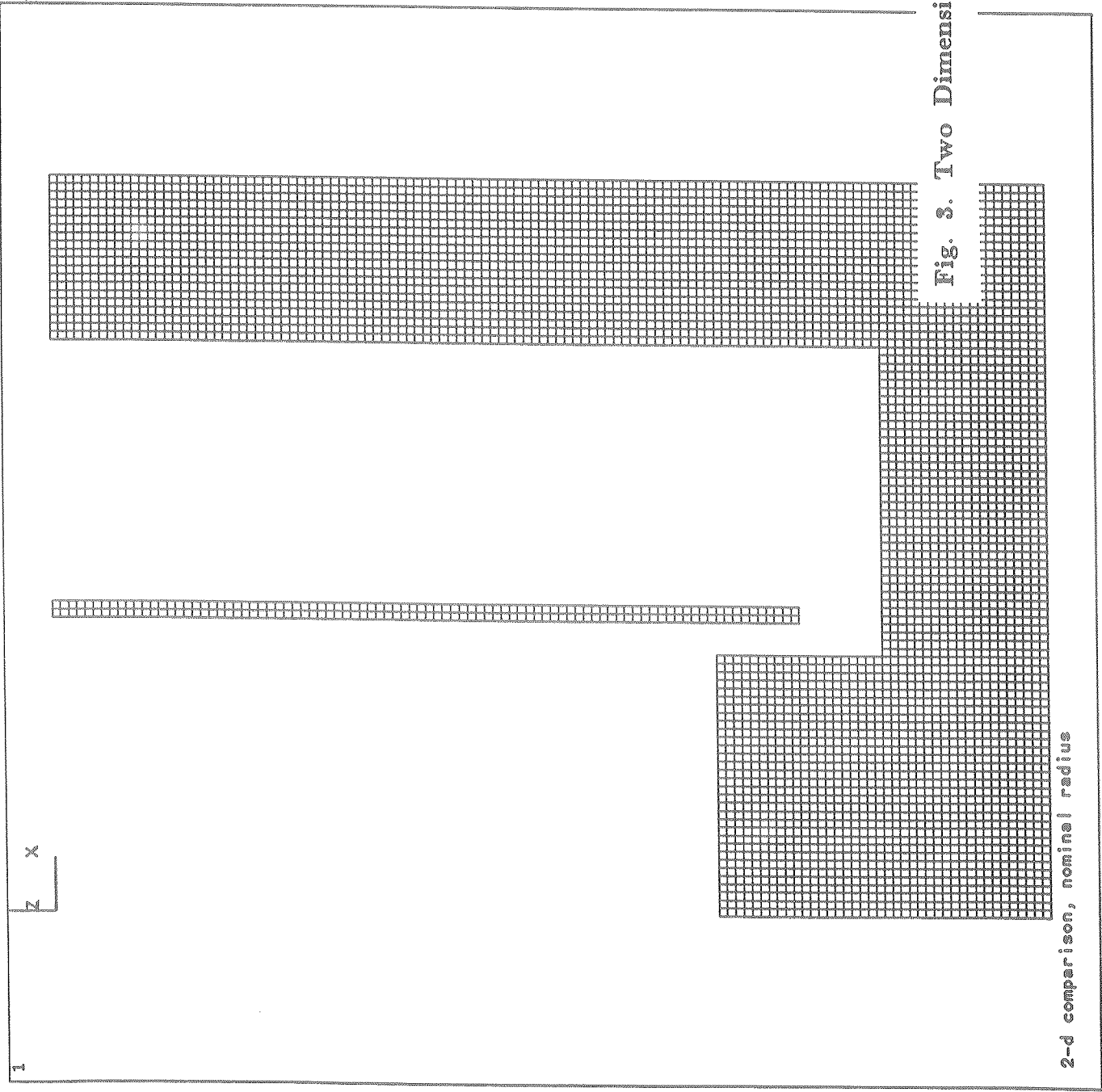


Fig. 3. Two Dimensional Axisymmetric Mesh

2-d comparison, nominal radius

ANSYS 4.4A
JUL 9 1991
8:03:30
PLOT NO. 1
POST1 ELEMENTS
TYPE NUM
XV =1
YV =1
ZV =1
DIST=6.726
YF =-3
ZF =-2.25
PRECISE HIDDEN

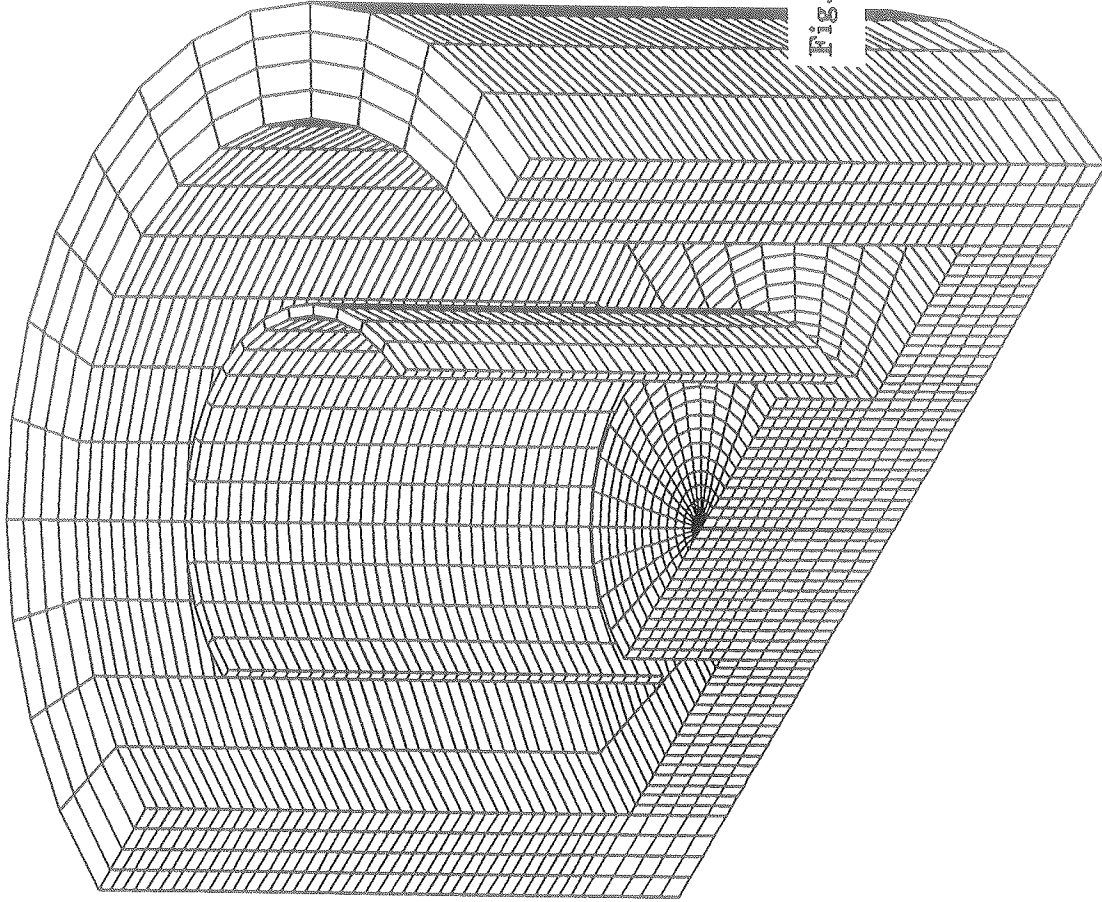


Fig. 4. Difference Scalar Potential Coarse Mesh

3-d difference potential coarse mesh (air removed for clarity)

ANSYS 4.4A
JUL 9 1991
9:19:02
PLOT NO. 1
POST1 ELEMENTS
TYPE NUM

XV =1
YV =1
ZV =1
DIST=3.84
YF =-2.4
ZF =-1.25
PRECISE HIDDEN

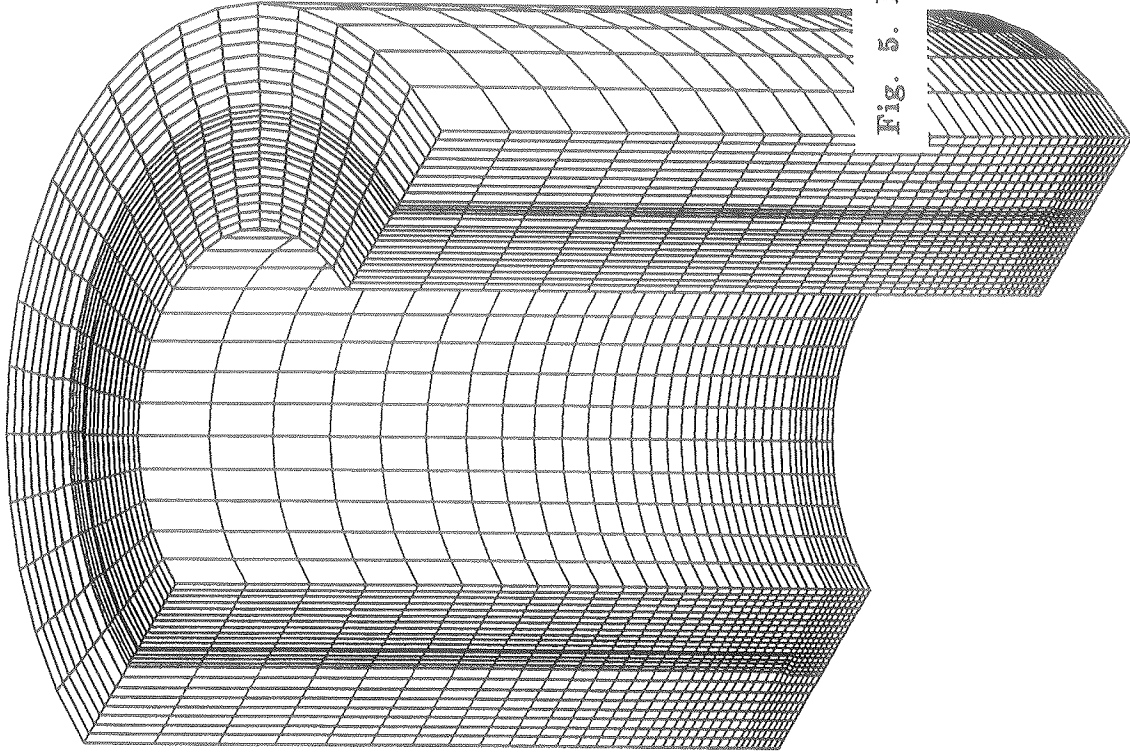
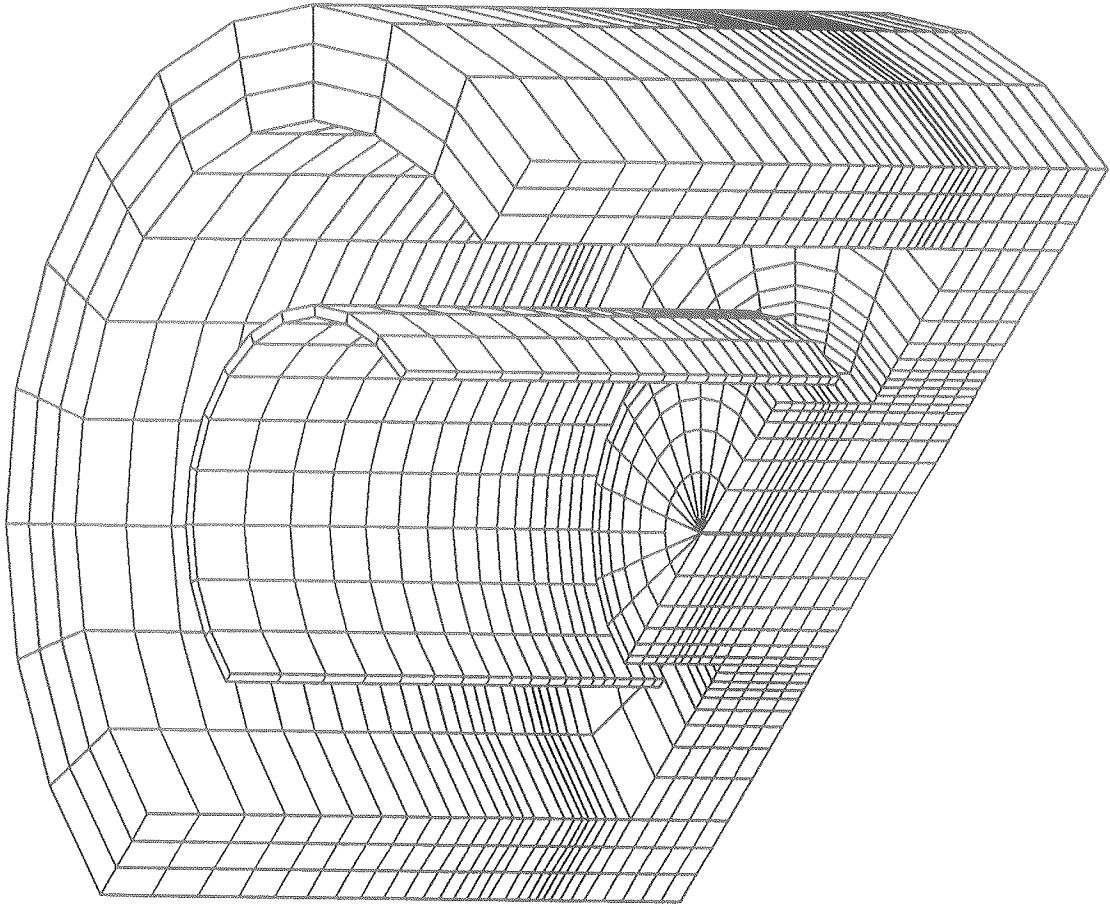


Fig. 5. Difference Scalar Potential Refined Submodel Mesh

3-d comparison, submodel, coil moved 2 cm in x

ANSYS 4.4A
JUL 8 1991
7:44:23
PLOT NO. 1
POST1 ELEMENTS
TYPE NUM

XV = 1
YV = 1
ZV = 1
DIST=5.726
YF = -3
ZF = -2.25
PRECISE HIDDEN



3-d vector potential coarse mesh (air removed for clarity)

Fig. 6. Vector Potential Coarse Mesh

ANSYS 4.4A
JUL 9 1991
8:47:11
PLOT NO. 1
POST1 ELEMENTS
TYPE NUM
XV =1
YV =1
ZV =1
DIST=3.84
YF =-2.4
ZF =-1.25
PRECISE HIDDEN

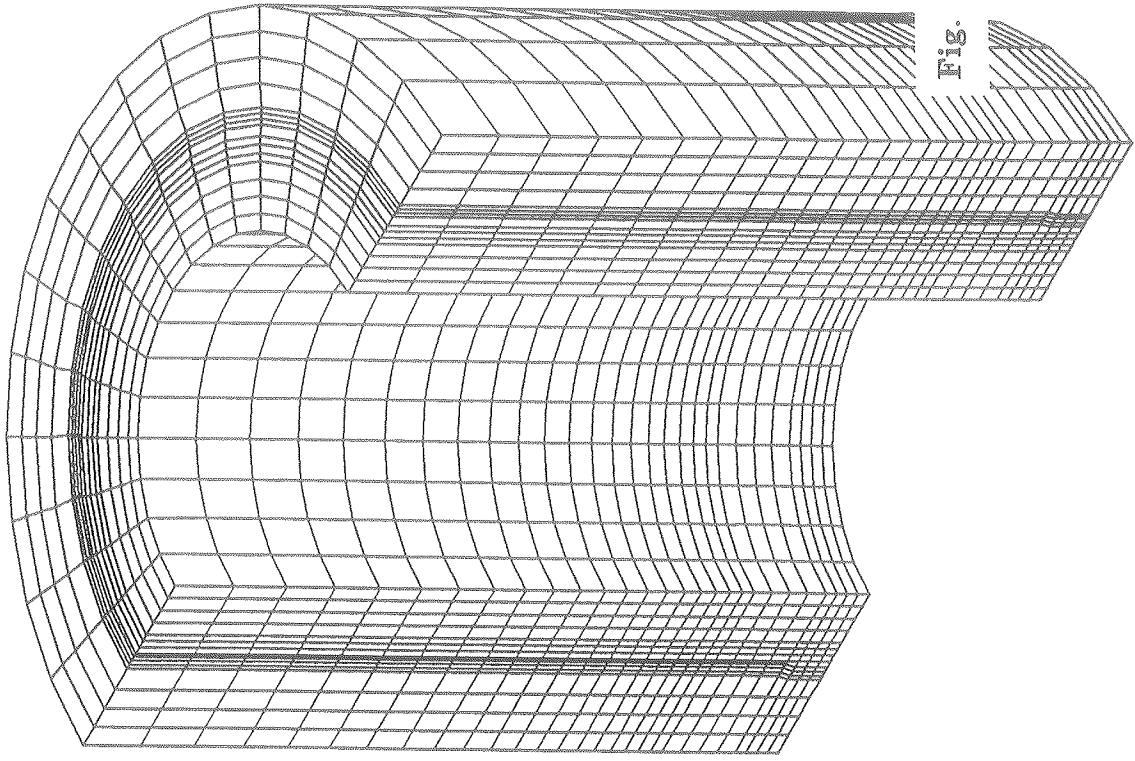


Fig. 7. Vector Potential Refined Submodel Mesh

3-d comparison, submodel, coil moved 2 cm in x, vect.pot.

Fig. 8.

Axial Field in Coil for Centered Coil

comparison of Difference and Vector Potentials

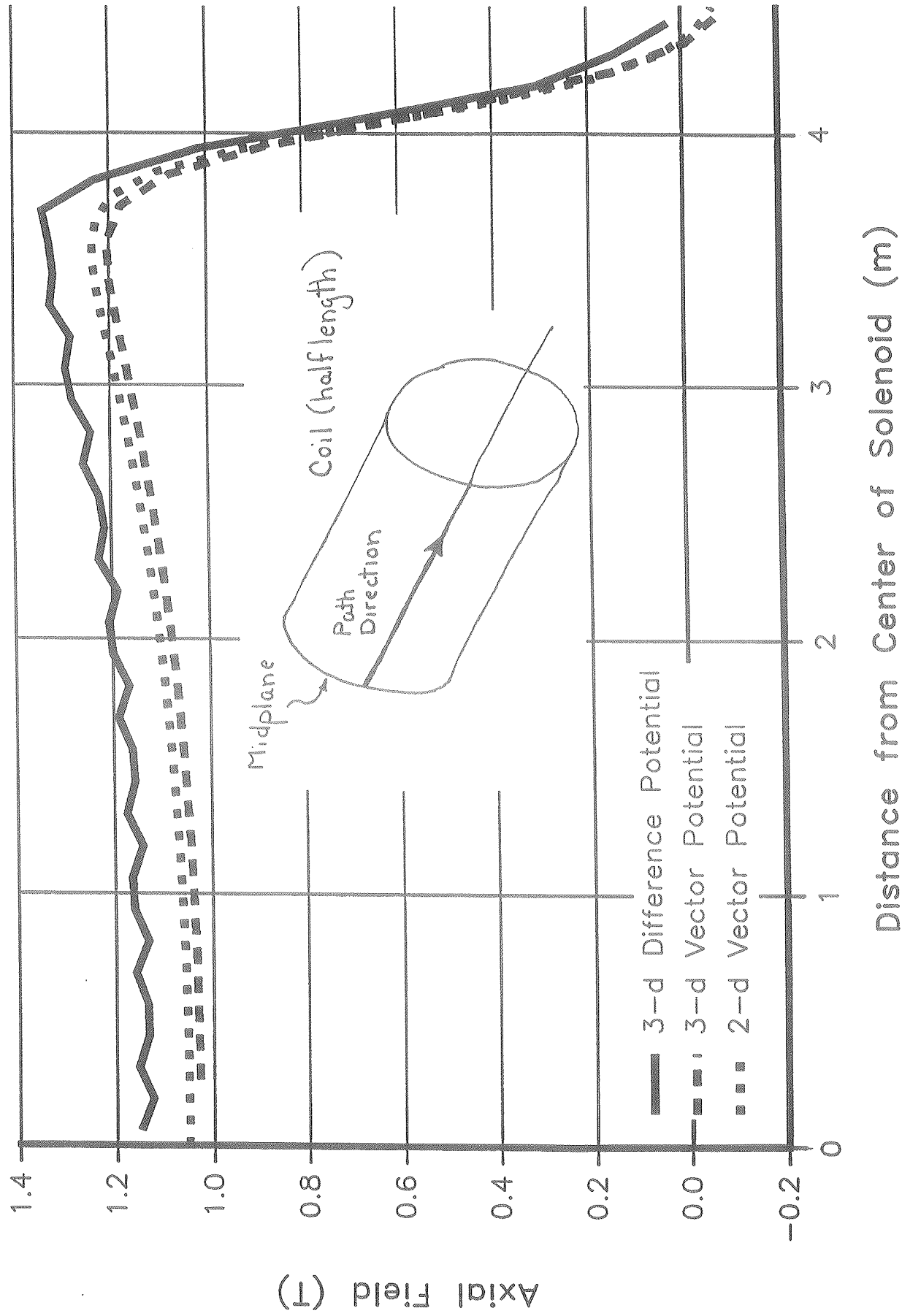
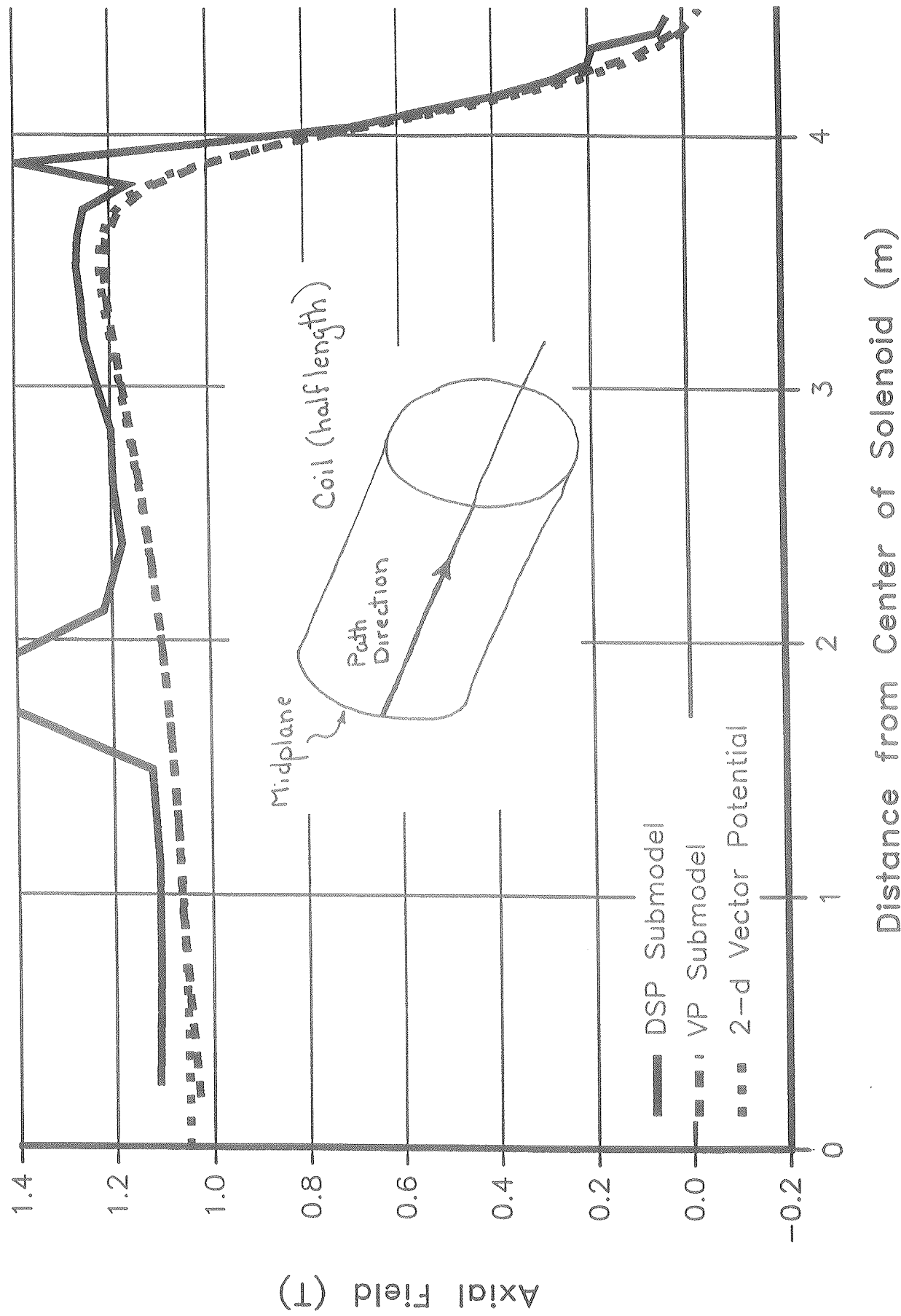


Fig. 9.

Axial Field in Displaced Coil for 3-d Submodels

comparison of Difference and Vector Potentials



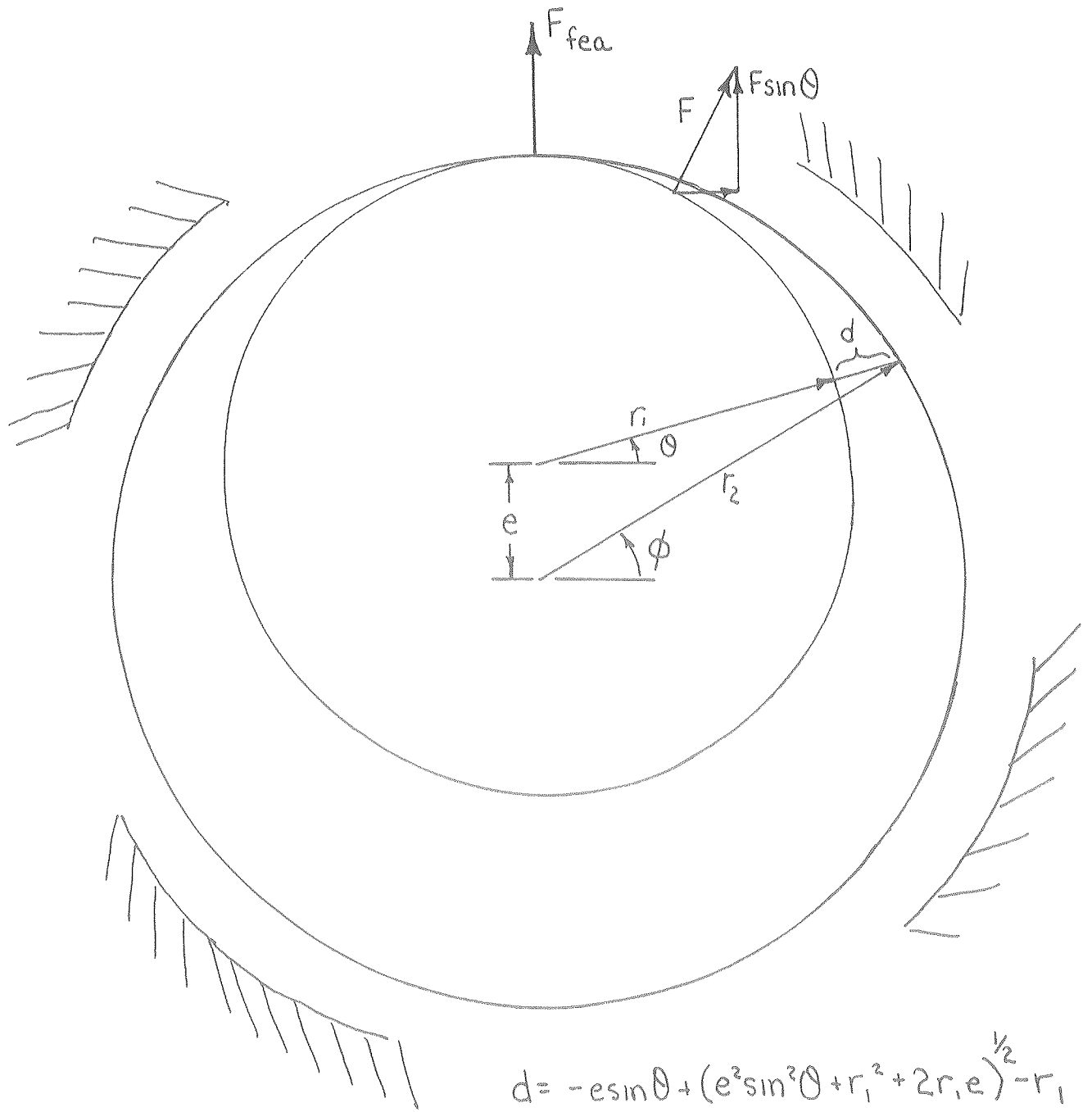


Fig A1

